Performance comparison of Division of Time and Division of Focal Plane polarimeters

Pierre-Jean Lapray[a] and Laurent Bigué[a]

[a]Université de Haute-Alsace, IRIMAS UR 7499, F-68100 Mulhouse, France

ABSTRACT

Two typical instruments can be employed for linear polarization imaging: a rotating polarizer in front of a classical monochrome camera (division of time), or a dedicated sensor with a polarization filter array (division of focal-plane). The last method enables the snapshot acquisition of the linear polarization properties of the light with a compact and affordable instrument. The rotating polarizer method has until now been preferred when good polarimetric precision is required. It is still unclear how these two techniques perform comparatively in terms of polarimetric accuracy. This paper provides a practical comparison between the two methods, and evaluates the effect of pre-processing applied on raw images to counterbalance the differences.

Keywords: Polarimetric imaging, Stokes imaging, Image denoising, Image capture, Sensors

1. INTRODUCTION

Polarization is the direction of oscillation of the electric field perpendicularly to the direction of propagation. The light can be fully, partially polarized (either linearly or circularly), or not polarized. An imaging polarimeter is an instrument capable to measure the state of polarization of light in 2D. Like spectral camera captures image data at specific wavelength ranges, a linear polarization camera filters the input at specific polarization angles. This enables computer vision tasks such as shape estimation,[1–3] or surface reflectance analysis.[4]

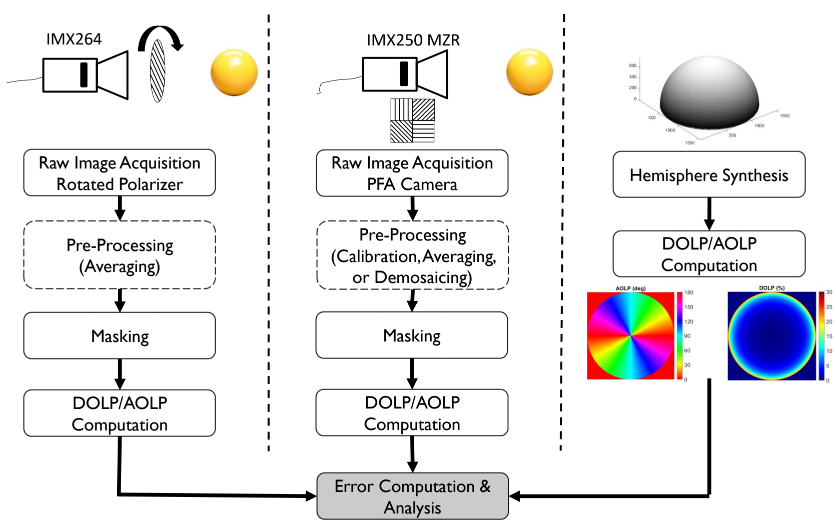

Figure 1: Diagram of the experiment of the paper, described in Section 3.

One of the first polarization imaging devices is the rotating polarizer,[5] used in a division-of-time (DoT) scheme.[6] It consists in the rotation of a full format polarizer in front of a conventional camera, and at different relative angles. This has the advantage to potentially use high quality polarizers (i.e. with a high extinction ratio) when needed. But this has several limitations, such as the size of the polarimeter, the cost of the optical/mechanical elements, or the inability to capture the information in a snapshot way.

Further author information: (Send correspondence to P.-J.L)
P.-J.L: E-mail: pierre-jean.lapray@uha.fr

Division of focal plane (DoFP) polarimetry is an emerging technique using a polarization filter array (PFA).[7] A spatial modulation in the focal-plane array permits to sample the intensities of the light field through several polarizing directions θ. The most common PFA camera embeds a 4-channel sensor,[8] which combines four angles of analysis, equally-distributed between 0° and 180° ($\theta = 0°, 45°, 90°, 135°$). The SONY IMX250 MZR,[9] exhibiting 5 Mpixels, is one practical instantiation and is commercially available, integrated by many camera manufacturers. Another even newer sensor version is the cheaper SONY IMX264 MZR sensor. This suggests that more applications using this technology will be introduced in the future. Nevertheless, compared to the rotating polarizer technique, this method suffers from additional noise. Like images produces with a Bayer filter array, PFA images need their spatial resolution to be reconstructed in order to avoid band registration errors. Extensive works were conducted on demosaicing PFA images.[10] PFA cameras also exhibit the noises inherent to silicon sensors, like temporal noise (which can be counterbalanced by frame averaging), but also polarization-specific noise due to optical imperfections introduced during micro-filter manufacturing and assembly (which can be counterbalanced by calibration[11,12]).

Unlike colour/spectral imaging, it is difficult to assess the performance of polarimetric sensors in practice, due to the lack of relevant and reproducible reference data. Nevertheless, a method for a quantitative evaluation of noise in polarimeters has been published by Atkinson et al.[3] This method uses a dielectric material, i.e. a snooker ball, illuminated by a point source at its normal. The sphere-theoretical reflection model allows the synthesis of reference data and the quantification of errors with respect to it. It was specifically used to benchmark the acquisition conditions (light source stability, spectral emission dependency, polarization type dependency, etc.), by comparing the polarimetric reconstruction results with respect to the theoretical expectation.[3] We believe that a similar method can be employed to investigate how the recent PFA cameras perform in terms of polarimetric precision compared to the rotated polarizer technique. Moreover, it can permit to evaluate how dedicated pre-processing applied to PFA images can potentially counterbalance these differences.

This paper has two distinct contributions:

1. A practical comparison between a division of time and a division of focal plane polarimeters, using the similar transducers. The sensors are the IMX264 and the IMX250 MZR respectively, where the second only differs from the first in that it has an additional PFA layer [*]. This allows a fair comparison between the noise introduced by polarizing elements.

2. A quantitative analysis on the effect of pre-processing applied to raw images: averaging, demosaicing, and calibration. The pre-processing effects are quantified in real conditions using a reference sphere as a sample, where a wide variety of degrees of polarization and signal intensities is obtained.

The paper is organized as follows. We first describe the related polarization imaging background in Section 2. Then, we define the experimental protocol in Section 3. Finally, results and analysis are provided in Section 4, before concluding in Section 5.

2. POLARIZATION BACKGROUND

2.1 Stokes measurement

The polarization state of the light is often represented by the Stokes formalism,[13] i.e. a four-component vector $\boldsymbol{S} = [S_0\ S_1\ S_2\ S_3]^t$. The total light intensity is S_0, S_1 is the intensity difference through 0° and 90° polarizers, S_2 the intensity difference through 45° and 135° polarizers, and S_3 referring to left or right-handed polarization components. In case of only sensing the linear state of polarization, the S_3 component is omitted. Assuming no additive noise in the polarimeter, the intensity measurement I through any optical element is related to the Stokes vector S by a linear combination as follows:

$$I = \mathbf{AS}\ , \tag{1}$$

[*]the performance of the IMX250 MYR and IMX264 sensors are the same, the major difference is only in the reduced frame rate.

where $\boldsymbol{A}$ is the analyser vector of the optical element at a specific polarization angle θ, which characterizes its polarimetric behaviour.

In the following, the optical element will be a linear polarizer with azimuth angle θ, considered as ideal ($\mathbf{A}_\theta = \mathbf{A}_{\theta,\mathbf{ideal}}$), i.e. the polarization element is perfect and exhibits high extinction ratios and high angular precision. For a typical 4-channel sensor with four ideal analysers oriented at $\theta = \{0°, 45°, 90°, 135°\}$ (angles are equally-spaced $\in [0, 180]\,°$), this leads to:

$$\boldsymbol{I} = \begin{bmatrix} I_0 \\ I_{45} \\ I_{90} \\ I_{135} \end{bmatrix} = \mathbf{W_{ideal}S} = \frac{1}{2}\begin{bmatrix} 1 & 1 & 0 & 0 \\ 1 & 0 & 1 & 0 \\ 1 & -1 & 0 & 0 \\ 1 & 0 & -1 & 0 \end{bmatrix}\begin{bmatrix} S_0 \\ S_1 \\ S_2 \\ S_3 \end{bmatrix}, \tag{2}$$

where the polarimetric measurement matrix $\boldsymbol{W}_{ideal}$ is defined with the rows containing the four analyser vectors $\boldsymbol{A}_\theta$. In case of nonidealities, the matrix $\boldsymbol{W}$ needs to be calibrated.[11,12]

The estimation of the Stokes vector $\hat{\boldsymbol{S}}$ is then done by using a pseudo-inverse estimator: $\hat{\boldsymbol{S}} = \boldsymbol{W}^{+}_{\boldsymbol{ideal}}\boldsymbol{I}$. More interpretable parameters can be derived from the recovered Stokes vector, i.e. the total intensity of input light $Int = S_0$, the degree of polarization $\rho \in [0, 100]\%$ (amount of polarized light over total intensity), and the angle of polarization $\phi \in [0, 180]°$:

$$Int = S_0 \qquad \rho = \frac{\sqrt{S_1^2 + S_2^2}}{S_0} \qquad \phi = 0.5 \arctan\left(\frac{S_2}{S_1}\right) \tag{3}$$

For a perfectly polarized light, $\rho = 1$, whereas for unpolarized light, $\rho = 0$. Reflection, scattering, or transmission usually change the state of polarization of an incident light beam.

2.2 Polarization Properties of Diffuse Reflected Light

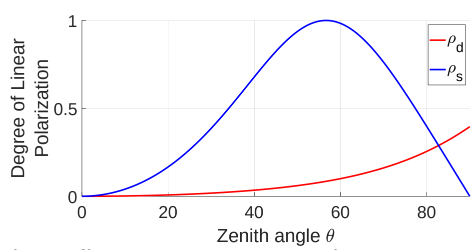

Figure 2: Degrees of polarization for different zenith angles for the two reflection types, either diffuse and specular, and for a refractive index of 1.52 (polyester).

The dichromatic reflection model predicts that the intensity of the light reflected from a surface is a linear combination of the specular and the diffuse reflection components.[14,15] The amount of polarized light upon reflection is modelled by the Fresnel reflection coefficients, which predicts the polarization of the reflected light in the directions perpendicular and parallel to the plane of incidence, and depend on the material properties (index of refraction), and the angle of incidence.[16] These dependencies have been exploited for diffuse/specular component separation,[17] shape reconstruction,[1] or material classification.[18] For a diffuse reflection, the degree of polarization is expressed as follows:[16,19]

$$\rho_d = \frac{(n - \frac{1}{n})^2 \sin^2\theta}{2 + 2n^2 - (n + \frac{1}{n})^2 \sin^2\theta + 4\cos\theta\sqrt{n^2 - \sin^2\theta}}, \tag{4}$$

where ρ_d is the degree of polarization of the diffuse reflected light, θ is the zenith angle (the angle between the viewing direction and the surface normal of the object), and n is the refractive index of the material. Figure 2 shows the degrees of polarization in the diffuse and specular reflection cases (ρ_d and ρ_s respectively), as a function

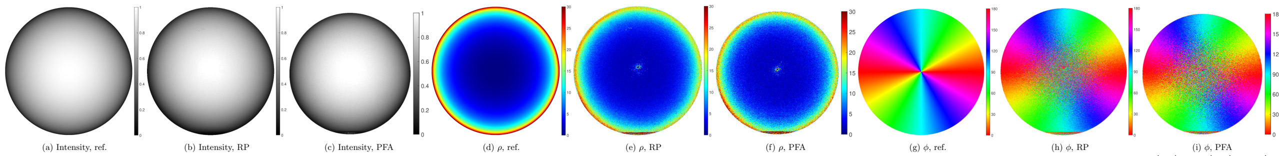

Figure 3: Intensity, degree of polarization ρ, and angle of polarization ϕ images computed from (a), (d), (g) sphere synthesis, (b), (e), (h) raw image from rotated polarizer (RP), and (c), (f), (i) raw image from PFA.

of the zenith angle θ for an air-polyester reflection. The resulting degree of polarization is generally lower for a diffuse reflection than a specular reflection, but obeys a one-to-one relationship with the zenith angle. Moreover, in case of diffuse reflection, the angle of polarization is equal to the azimuth angle Φ, whereas it is perpendicular to it for the specular reflection.

2.3 Hemisphere synthesis

To compare the accuracy of both acquisition systems, we use a ground truth object with a known shape (therefore known zenith and azimuth angles), i.e. a sphere. This has the advantage of having reference data for a wide range of angles and degrees of polarization. We synthesize the coordinates of points on a three-dimensional hemisphere by:

$$\begin{bmatrix} x \\ y \\ z \end{bmatrix} = \begin{bmatrix} r\sin\theta\cos\phi \\ r\sin\theta\sin\phi \\ r\cos\theta \end{bmatrix} , \tag{5}$$

where x, y, and z are the Cartesian coordinates, θ and ϕ are the spherical coordinates ($0 < \theta < \frac{\pi}{2}$ and $0 < \phi < 2\pi$), and r is the radius of the sphere in number of pixels. The radius and center of the synthesized hemisphere are adjusted relatively to the radius and center of the snooker ball image captured in the experiment (see Section 3). We also compute the 3D surface normal components p_x, p_y, and p_z from the surface coordinates (with *surfnorm* function in Matlab). Then, we can compute the corresponding polarization images properties Int_{ref}, ρ_{ref}, and ϕ_{ref} of the hemisphere as follows:

- $Int_{ref} = p_z$, because for a Lambertian surface with coincident light source and camera and unit albedo, the intensity is equal to the z-component of the surface normal (p_z).
- $\rho_{ref} = \rho_d$, the degree of polarization computed from Eq. 3 (assuming no specular reflection).
- $\phi_{ref} = \frac{\pi}{2} + \arctan\frac{p_x}{p_y}$

The resulting 3D synthesized hemisphere images are shown in Figure 1, and reference images are shown in Figures 3a, 3d, and 3g.

3. EXPERIMENTAL PROTOCOL

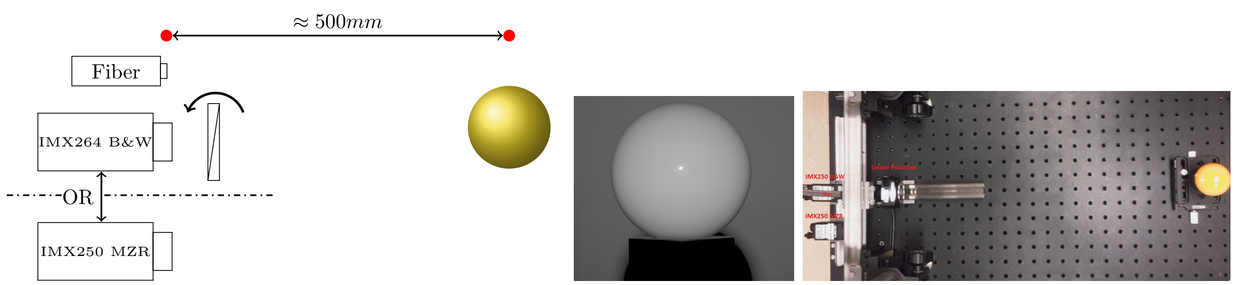

(a) (b) (c)

Figure 4: (a) Acquisition setup schematic, (b) scene visualization, and (c) setup picture. Acquisition is done with one camera at a time, where both cameras are interchangeable with mechanical rails.

We compare the polarimetric results from two different acquisition systems, and see how pre-processing applied to PFA is affecting the error computed on a reference sphere.

3.1 Acquisition of images

The experimental setup is shown in Figure 4a. Two different imaging polarimeters are considered:

1. **Rotating Polarizer (RP)**: a camera with the SONY IMX264 monochrome sensor (TRI050S camera manufactured by LUCID Vision Labs Inc.), with a 1" 10LP-VIS-B linear polarizer (mounted on a CONEX-AG-PR100P motorized rotary stage from Newport) rotated in front of it. The polarizer is mounted on a precise motorized rotational stage, and is considered as a high-quality polarizer.

2. **Polarization Filter Array camera (PFA)**: a camera with the SONY IMX250 MZR sensor (TRI050S-P camera manufactured by LUCID Vision Labs Inc.), with embedded grid of polarization micro-filters.

The two cameras are equipped with a $50mm$ camera lens (Navitar MVL50M23), whose aperture is fixed at $f/5.6$. All the embedded processings inside the cameras have been disabled, such as auto-gain or auto-exposure. The exposure time is fixed at $20ms$ for both cameras.

For the sphere, we installed a yellow-orange snooker ball (diameter $50mm$), from which we assume that it has a perfect shape, at a distance from the camera of $\approx 50cm$. The index of refraction is assumed to be 1.52 (polyester).

3.2 Pre-processing

In this work, we consider three types of noise that can occur in polarimeters: signal dependent noise (temporal noise), imperfection of polarizers, and spatial registration noise. These can be partially counterbalanced by processing applied to raw images. We study the effect of these processing in polarimetric accuracy.

Averaging Temporal noise is signal dependent noise that can be counteracted by averaging. We propose to acquire multiple times the same signal and average the corresponding 2, 4, 10, 50, and 100 images. We do the same averaging for the two polarimeters tested in this work for comparison.

Calibration Calibration algorithms have been recently developed and adapted to the PFA instruments. We implement the single pixel and superpixel techniques,[11,12] which are the most popular algorithms to calibrate polarimetrically the PFA images. The result of the calibration for the PFA camera used in this work is shown in Figure 5. In the related works, the polarimetric error before and after calibration is evaluated using a spatially uniform and fully polarized lighting (e.g. an integrating sphere),[11,20,21] but never on textured objects.

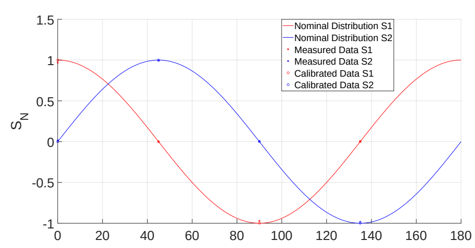

Figure 5: Results of the polarimetric calibration (super-pixel method) for a group of 2×2 pixels at the center of the PFA sensor. The single pixel method gives very similar results, which are omitted.

Demosaicing We selected four demosaicing algorithms to evaluate them with respect to the proposed experiment. The first two are not PFA-specific and commonly used for color demosaicing, while the last two are the last state-of-the-art algorithms dedicated to PFA images: 1-Bilinear (noted B),[22] 2-Bicubic-spline (BCSP),[23] 3-Edge-Aware Residual Interpolation (EARI):[24] a filtering-based technique dedicated to the specific case of PFA, 4-Alternating Direction Multipliers Minimization (ADMM):[25] an adaptation of the ADMM framework to the polarization case, to recover directly the unknown Stokes vectors from an optimization problem on a dataset. We used the available model without retraining the model.

4. RESULTS AND ANALYSIS

Table 1: Evaluation of RT and PFA-based polarimeters in terms of polarization errors (mean μ and standard deviation σ) for various pre-processing. E_ρ and E_Φ are expressed in % and degrees, respectively.

	Rotated Polarizer		PFA	
	E_ρ (μ/σ)	E_ϕ (μ/σ)	E_ρ (μ/σ)	E_ϕ (μ/σ)
Raw				
1 image	1.95/2.86	14.0/18.1	2.01/2.71	15.0/18.7
Averaging				
2 images	1.61/2.78	11.4/16.5	1.65/2.62	12.5/17.1
4 images	1.39/2.76	9.3/15.0	1.43/2.58	10.6/15.7
10 images	1.21/2.76	7.3/13.3	1.26/2.56	9.0/14.4
50 images	1.07/2.77	5.4/11.6	1.14/2.56	7.8/13.2
100 images	1.04/2.77	4.8/11.1	1.13/2.56	7.7/13.0
Calibration				
Single-pixel cal.[11]	-	-	2.00/2.75	14.80/18.68
Super-pixel cal.[11]	-	-	2.00/2.74	14.77/18.65
Demosaicing				
Bilinear[22]	-	-	1.71/2.66	12.45/17.35
Bicubic-spline[23]	-	-	1.89/2.80	13.76/18.13
EARI[24]	-	-	1.49/2.61	10.69/16.24
ADMM[25]	-	-	1.04/2.70	5.76/12.23

We evaluated the imaging results relatively to the reference sphere synthesized in Section 2.3. In Table 1, we summarized the mean and standard deviation errors in ρ et ϕ images, for raw, averaged, calibrated, and demosaiced data. The evaluation is done on pixels pertaining to the region of interest defined by the complete hemisphere, and omitting the background.

We can see that the two setups are very close in terms of polarimetric errors when we do not perform any temporal averaging. As the two setups use the same transducers, the difference in errors can be assumed to be induced only by the polarizers. For the RP setup, even if the polarizer is assumed to be perfect, the remaining polarimetric errors for RP method can be explained by the sensor noise (photon shot, quantification, and Poisson noises) which induces polarimetric noise. As the transducers are the same, all the sources of noise induced in RP setup are present in PFA setup. One could have imagined a larger difference between the two setups. This suggests that micropolarizer manufacturing (especially with this SONY Polarsense technology) has reached a great maturity, which was not the case for previous PFA-based polarimeters.[11] The small difference in errors in the raw PFA and RP data can be explained by the fact that the micropolarizer array still contains some manufacturing imperfections which affect the polarization efficiency.

We can see that a little improvement in the errors is encountered when calibration is applied to PFA images. This decreases the error on ρ and ϕ by 6% and 1.5% respectively. As explained in,[11] there are some imperfections in the manufacturing process of micro-polarizer array, i.e. non-ideal diattenuation, spatial variation of polarizer orientations, cross-talk effect, misalignment of the PFA with respect to the focal-plane array, etc. Moreover, the results show a very small difference between the two calibration techniques, suggesting that there is no need to calibrate these PFA images using a 2×2 neighborhood (a superpixel). It is known that the superpixel calibration only shows an advantage when the four polarization responses need to be aligned relatively.[11] This seems to be not the case with these recent PFA devices, where the angles of polarizers are precise and uniform.

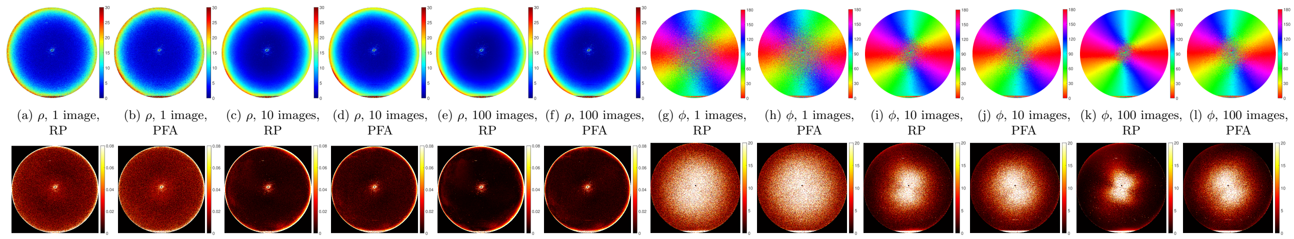

(a) ρ, 1 image, RP (b) ρ, 1 image, PFA (c) ρ, 10 images, RP (d) ρ, 10 images, PFA (e) ρ, 100 images, RP (f) ρ, 100 images, PFA (g) ϕ, 1 images, RP (h) ϕ, 1 images, PFA (i) ϕ, 10 images, RP (j) ϕ, 10 images, PFA (k) ϕ, 100 images, RP (l) ϕ, 100 images, PFA

(m) Error map ρ, 1 image, RP (n) Error map ρ, 1 image, PFA (o) Error map ρ, 10 images, RP (p) Error map ρ, 10 images, PFA (q) Error map ρ, 100 images, RP (r) Error map ρ, 100 images, PFA (s) Error map ϕ, 1 images, RP (t) Error map ϕ, 1 images, PFA (u) Error map ϕ, 10 images, RP (v) Error map ϕ, 10 images, PFA (w) Error map ϕ, 100 images, RP (x) Error map ϕ, 100 images, PFA

Figure 6: Varying the number of averaged frames. Visualization of ρ, ϕ and error maps for both RP and PFA instruments.

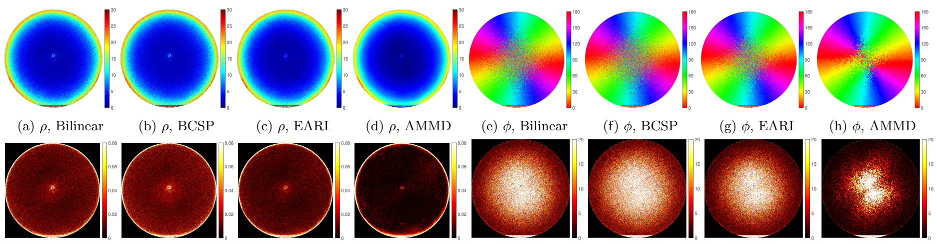

(a) ρ, Bilinear (b) ρ, BCSP (c) ρ, EARI (d) ρ, AMMD (e) ϕ, Bilinear (f) ϕ, BCSP (g) ϕ, EARI (h) ϕ, AMMD

(i) Error map ρ, Bilinear (j) Error map ρ, BCSP (k) Error map ρ, EARI (l) Error map ρ, ADMM (m) Error map ϕ, Bilinear (n) Error map ϕ, BCSP (o) Error map ϕ, EARI (p) Error map ϕ, ADMM

Figure 7: Varying the demosaicing methods for single PFA frames.

By looking at the PFA demosaicing results (Table 1 and Figure 7), especially the learning-based algorithms, we see that the demosaicing helps to smooth the polarimetric parameters spatially. For the Qiu et al. method,[25] the error is even lower compared to RP method averaged 100 times. This means that the algorithm acts as a denoising procedure, i.e a smoothing function in the polarimetric domain. These results are only verified for this type of data, mainly containing low spatial frequencies (i.e. the sphere surface). This needs to be confirmed for data containing high frequencies.

By looking at the results before and after averaging (Table 1 and Figure 6), we see that the error decreases similarly for the two setups when we average the intensities.

5. CONCLUSION

We investigated the noise and the pre-processing applied to a polarization filter array polarimeter, as compared to the performance of a rotated polarimeter. We used reference data computed from the sphere-theoretical reflection model, which allows the synthesis of reference data and the quantification of errors with respect to it. We have found that the two setups are very closed, which suggests that the micropolarizer manufacturing has reached a great maturity, unlike previous PFA-based polarimeters. We also found that the dedicated PFA-demosaicking algorithms can greatly reduce the polarimetric errors for reconstructing low spatial frequencies, and that polarimetric calibration achieves a relatively small improvement.

ACKNOWLEDGMENTS

This work was supported by the ANR JCJC SPIASI project, grant ANR-18-CE10-0005 of the French Agence Nationale de la Recherche.

REFERENCES

[1] Miyazaki, Tan, Hara, and Ikeuchi, "Polarization-based inverse rendering from a single view," in [*Proceedings Ninth IEEE International Conference on Computer Vision*], 982–987 vol.2 (2003).

[2] Morel, O., Stolz, C., Meriaudeau, F., and Gorria, P., "Active lighting applied to three-dimensional reconstruction of specular metallic surfaces by polarization imaging," *Appl. Opt.* **45**, 4062–4068 (Jun 2006).

[3] Atkinson, G. A., Thornton, T. J., Peynado, D. I., and Ernst, J. D., "High-precision polarization measurements and analysis for machine vision applications," in [*2018 7th European Workshop on Visual Information Processing (EUVIP)*], 1–6 (2018).

[4] Riviere, J., Reshetouski, I., Filipi, L., and Ghosh, A., "Polarization imaging reflectometry in the wild," *ACM Trans. Graph.* **36** (nov 2017).

[5] Walraven, R., "Polarization Imagery," *Optical Engineering* **20**(1), 14 – 18 (1981).

[6] Tyo, J. S., Goldstein, D. L., Chenault, D. B., and Shaw, J. A., "Review of passive imaging polarimetry for remote sensing applications," *Appl. Opt.* **45**, 5453–5469 (Aug 2006).

[7] Rust, D. M., "Integrated dual imaging detector," (Aug. 1 1995). US Patent 5,438,414.

[8] Chun, C. S., Fleming, D. L., and Torok, E., "Polarization-sensitive thermal imaging," in [*Automatic Object Recognition IV*], **2234**, 275–286, International Society for Optics and Photonics (1994).

[9] Sony, "Polarization image sensor," tech. rep., Polarsens (2018).

[10] Mihoubi, S., Lapray, P.-J., and Bigué, L., "Survey of demosaicking methods for polarization filter array images," *Sensors* **18**(11) (2018).

[11] Powell, S. B. and Gruev, V., "Calibration methods for division-of-focal-plane polarimeters," *Opt. Express* **21**, 21039–21055 (Sep 2013).

[12] Giménez, Y., Lapray, P.-J., Foulonneau, A., and Bigué, L., "Calibration algorithms for polarization filter array camera: survey and evaluation," *Journal of Electronic Imaging* **29**(4), 1 – 13 (2020).

[13] Stokes, G. G., "On the composition and resolution of streams of polarized light from different sources," *Transactions of the Cambridge Philosophical Society* **9**, 399 (1851).

[14] Torrance, K. E. and Sparrow, E. M., "Theory for off-specular reflection from roughened surfaces∗," *J. Opt. Soc. Am.* **57**, 1105–1114 (Sep 1967).

[15] Shafer, S. A., "Using color to separate reflection components," *Color Research & Application* **10**(4), 210–218 (1985).

[16] Born, M. and Wolf, E., [*Principles of optics: electromagnetic theory of propagation, interference and diffraction of light*], Elsevier (2013).

[17] Nayar, S. K., Fang, X.-S., and Boult, T., "Separation of reflection components using color and polarization," *International Journal of Computer Vision* **21**(3), 163–186 (1997).

[18] Tominaga, S. and Kimachi, A., "Polarization imaging for material classification," *Optical Engineering* **47**(12), 1 – 14 (2008).

[19] Wolff, L. and Boult, T., "Constraining object features using a polarization reflectance model," *IEEE Transactions on Pattern Analysis and Machine Intelligence* **13**(7), 635–657 (1991).

[20] Lane, C., Rode, D., and Rösgen, T., "Calibration of a polarization image sensor and investigation of influencing factors," *Appl. Opt.* **61**, C37–C45 (Feb 2022).

[21] Hagen, N. A., Shibata, S., and Otani, Y., "Calibration and performance assessment of microgrid polarization cameras," *Optical Engineering* **58**(8), 1 – 9 (2019).

[22] Ratliff, B. M., LaCasse, C. F., and Tyo, J. S., "Interpolation strategies for reducing ifov artifacts in microgrid polarimeter imagery," *Optics express* **17**(11), 9112–9125 (2009).

[23] Gao, S. and Gruev, V., "Bilinear and bicubic interpolation methods for division of focal plane polarimeters," *Opt. Express* **19**, 26161–26173 (Dec 2011).

[24] Morimatsu, M., Monno, Y., Tanaka, M., and Okutomi, M., "Monochrome and color polarization demosaicking using edge-aware residual interpolation," in [*2020 IEEE International Conference on Image Processing (ICIP)*], 2571–2575 (2020).

[25] Qiu, S., Fu, Q., Wang, C., and Heidrich, W., "Linear polarization demosaicking for monochrome and colour polarization focal plane arrays," *Computer Graphics Forum* **40**(6), 77–89 (2021).